

Review

Metasurface Holography in the Microwave Regime

Guanyu Shang¹, Zhuochao Wang¹, Haoyu Li¹, Kuang Zhang² , Qun Wu², Shah Nawaz Burokur³ 
and Xumin Ding^{1,4,*}

¹ Advanced Microscopy and Instrumentation Research Center, Harbin Institute of Technology, Harbin 150080, China; 19B901010@stu.hit.edu.cn (G.S.); zhuochao_wang@hit.edu.cn (Z.W.); lihaoyu@hit.edu.cn (H.L.)

² Department of Microwave Engineering, Harbin Institute of Technology, Harbin 150001, China; zhangkuang@hit.edu.cn (K.Z.); qwu@hit.edu.cn (Q.W.)

³ LEME, UPL, Univ Paris Nanterre, F92410 Ville d'Avray, France; sburokur@parisnanterre.fr

⁴ Key Laboratory of Millimeter Waves, Southeast University, Nanjing 210096, China

* Correspondence: xuminding@hit.edu.cn

Abstract: Hologram technology has attracted a great deal of interest in a wide range of optical fields owing to its potential use in future optical applications, such as holographic imaging and optical data storage. Although there have been considerable efforts to develop holographic technologies using conventional optics, critical issues still hinder their future development. A metasurface, as an emerging multifunctional device, can manipulate the phase, magnitude, polarization and resonance properties of electromagnetic fields within a sub-wavelength scale, opening up an alternative for a compact holographic structure and high imaging quality. In this review paper, we first introduce the development history of holographic imaging and metasurfaces, and demonstrate some applications of metasurface holography in the field of optics. We then summarize the latest developments in holographic imaging in the microwave regime. These functionalities include phase- and amplitude-based design, polarization multiplexing, wavelength multiplexing, spatial asymmetric propagation, and a reconfigurable mechanism. Finally, we conclude briefly on this rapidly developing research field and present some outlooks for the near future.

Keywords: metasurface; holography; microwave



Citation: Shang, G.; Wang, Z.; Li, H.; Zhang, K.; Wu, Q.; Burokur, S.N.; Ding, X. Metasurface Holography in the Microwave Regime. *Photonics* **2021**, *8*, 135. <https://doi.org/10.3390/photonics8050135>

Academic Editor:
Pierre-Alexandre Blanche

Received: 29 March 2021
Accepted: 20 April 2021
Published: 22 April 2021

Publisher's Note: MDPI stays neutral with regard to jurisdictional claims in published maps and institutional affiliations.



Copyright: © 2021 by the authors. Licensee MDPI, Basel, Switzerland. This article is an open access article distributed under the terms and conditions of the Creative Commons Attribution (CC BY) license (<https://creativecommons.org/licenses/by/4.0/>).

1. Introduction

Holography was first invented by Dennis Gabor in 1948, as a method to produce a three dimensional image of an object [1]. In order to improve the resolution of electron microscopes and solve particular technical problems such as electron lens aberrations, Dennis Gabor used the transmission and reflection characteristics of photographic film to record the interference pattern of the incident wave and the object wave, realizing the analysis of the object wave image. With the development of laser technology in 1960, holographic imaging technology has rapidly developed in the optical field [2,3] due to powerful arbitrary beam shaping and predesigned image recording, and as such, reconstruction capabilities have progressed tremendously. However, traditional holographic imaging technology mainly uses specific nonlinear optical materials to record the interference light intensity of the incident wave and the object wave. In 1985, Sirat and Psaltis [4] presented a holographic system based on the properties of optical propagation in birefringent media, and named it conoscopic holography. Specifically, the reported conoscopic image is obtained when observing a spherical wave passing through a birefringent crystal through a crossed polarizer. In 1999, a novel form of microscopy known as coherent diffraction imaging (CDI) or lensless imaging was developed for the imaging of small-sized two-dimensional (2D) or three-dimensional (3D) structures [5]. However, such imaging systems using laser light sources not only necessitate extremely high environmental requirements, but also produce speckle noise and parasitic interferences, which cannot be applied to the field of

white (incoherent) light, and these factors greatly limit the application of traditional optical holographic imaging. Based on the above consideration, incoherent holography can solve this problem well. In 1961, Mertz and Young [6] proposed the method of zone-plate-coded holographic imaging. The emergence of incoherent holography means that the holographic recording process no longer relies on coherent light sources, and since then holography has been developed and applied rapidly. Kim et al. [7] analyzed the incoherent hologram generated by a triangular interferometer, and studied the imaging resolution of a triangular digital hologram. The most striking technology was introduced by Rosen et al. [8], who proposed Fresnel incoherent correlation holography (FINCH). FINCH exhibits a modulation transfer function (MTF) of which the width is twice of that of any coherent imaging system with the same numerical aperture, and unlike regular imaging systems, it has a uniform response to all frequencies below the cutoff frequency. In reference [9], it was shown that FINCH can record multi-color digital holograms of fluorescent objects. Later, Rosen further proposed a new incoherent self-informative-reference digital holography system with an improved axial resolution, dubbed ‘coded aperture correlation holography’ (COACH) [10]. This was the first time that the random-like phase masks were utilized as coded apertures in incoherent holography systems. Moreover, Kim et al. [11] presented the incoherent digital holography (IDH) scheme. Two concave (convex) mirrors with different curvatures were employed instead of the spatial modulator in the FINCH system as the diffractive beam-splitting element, enabling it to get rid of the limitation of the spatial modulator resolution on imaging, and to improve the imaging resolution of the system. Confocal incoherent correlation holography (CINCH) was proposed for the simultaneous real-time image capture of wide field and holographic images, or of confocal holographic images for the ready comparison of each method on the exact same field of view [12]. The successful achievement of the holographic recording and reconstruction of a natural outdoor scene with a holographic camera based on self-interference incoherent digital holography (SIDH) was also reported [13]. The utilization of volumetric holograms as imaging elements has been widely considered and a confocal imaging principle was proposed, in which matched filtering by a volume hologram was used instead of a pinhole filter [14].

On the basis of traditional holographic imaging technology, Brown and Lohman proposed the concept of computer-generated holography (CGH) in 1966 [15]. CGH is generated by diffraction calculations, projecting 2D or 3D objects as a virtual CGH hologram on the computer. Compared to traditional holographic imaging technology, computational holography transforms the problem of object image information reconstruction into the solution of hologram electric field distribution. The diffraction efficiency can be effectively increased by optimizing the solution algorithm [16]. In addition, the hologram of computer-generated holography (CGH) can be quickly obtained through numerical simulations, such that virtual images that do not exist in nature can be realized, which greatly increases the design freedom [17,18]. With its rapid development, holography technology has played an important role in three-dimensional display, data storage, measurement, biological image processing, and other fields. Traditional diffractive optical elements have first-order lenses, and the optical power is highly dependent on the wavelength. In order to address such an issue, Faklis et al. [19] proposed multi-order diffractive (MOD) Fresnel lenses to change the focused wavelength region by selecting the integral order. Thus, a MOD lens can provide high-quality imaging in broadband or multispectral illumination over wide fields of view. Golub et al. [20] designed a set of eight transmissive resonance-domain diffractive optical elements (DOEs) for multi-stripe structured illumination at visible wavelengths. The multifunctional DOEs comprise imaging, shaping, and multiplexing functions in a single binary surface relief layer. Roberts et al. [21] found that the combination of cycloidal diffractive waveplates (CDWs) and polarization volume gratings (PVGs) results in high-efficiency polarization-insensitive diffraction, which can be used in diffractive waveplate lenses. Furthermore, a polarization-independent liquid crystal Pancharatnam–Berry (PB) lens system [22] has been developed. By using at least four PB lenses with specific distances, the system manifests the same optical function for all polarizations.

However, since conventional phase holograms rely on light propagation over distances much longer than the wavelength, in order to accumulate enough phase variation for effective wavefront shaping, the optical elements for building the phase hologram will have large unit cell sizes due to the limited refractive indices of natural materials. Therefore, it is highly desired to fully manipulate the hologram with a device that possesses excellent performance and multiple functionalities.

Nowadays, the progress in nanofabrication techniques may revolutionize the method of achieving optical holography. A metasurface, as a two-dimensional (2D) version of a metamaterial, is typically a periodic, quasi-periodic or random array of sub-wavelength antennas composed of metal or dielectric structures with specific geometric shapes. Because of its unique ability to arbitrarily modulate the phase, amplitude and polarization of electromagnetic waves through a sub-wavelength-scale planar nanostructure, it has a small footprint and powerful versatility to produce various special optical effects. It has received extensive attention and has rapidly developed into a research field [23–28]. Compared to traditional optical elements and metamaterials, a metasurface presents the advantages of reduced absorption loss, relatively low manufacturing difficulty, being ultra-thin, and having an ultra-small pixel size for integration with on-chip nanophotonic devices. Hence, metasurfaces have produced breakthrough phenomena in the fields of electromagnetism and photonics. Because the metasurface is an artificially constructed material with design flexibility, it provides a new perspective for the design of various optical systems, such as the generation of vortex beams [29–31], data storage [32,33], encryption and anticounterfeiting [34,35], metalens and decentralized control [36–38], asymmetric transmission [39–41], nonlinear optics [42–44] and many more. One cutting-edge nanotechnology combines holography with metasurfaces. This metasurface holography can be achieved by accurately mapping the structure to the position and local scattering characteristics of the nano-scale optical resonators formed on the interface.

In the current work, we first review the emerging applications of metasurface holography in the optical regime. Then, we mainly focus our attention on the latest developments of metasurface holography in the microwave field, such as phase- and amplitude-based designs, polarization multiplexing, wavelength multiplexing, spatial asymmetric propagation, and reconfigurable technology. Finally, we put forward prospects and potential development directions associated with metasurface technology.

2. Optical Metasurface Holography

Early meta-holography studies exploited the Pancharatnam–Berry (PB) phase control method, which modulates the transmitted (or reflected) wavefront on the hologram by inducing the designated PB geometric phase factor associated with the polarization variation of light. By combining this with Poincaré sphere theory, it is possible to analyze the mechanism of obtaining the required phase mutation through the PB phase [45,46]. In order to quantify the relationship between space-variant polarization modification and the phase change, it has been shown that the phase factor (PF) is equal to half of the area that is encompassed by the loop on the Poincaré sphere, and its absolute value can be calculated as $PF = |2(\theta_1 - \theta_2)|$, assuming that the polarization changes from purely RCP to LCP, or vice versa, between the two poles of the sphere [47]. With arbitrary polarization rotation, any desired phase modification in the range $[0, 2\pi]$ can thus be achieved. Using the Jones matrix, the transmitted field of the PB elements can be calculated for arbitrarily polarized incident waves, as:

$$\left| \vec{E}_{out} \right\rangle = \sqrt{\eta_E} \left| \vec{E}_{in} \right\rangle + (\sqrt{\eta_R} e^{\pm i2\theta} \left| \vec{R} \right\rangle + \sqrt{\eta_L} e^{\pm i2\theta} \left| \vec{L} \right\rangle) \quad (1)$$

where $\eta_E = \left| \frac{1}{2}(t_x + t_y e^{i\phi}) \right|^2$, $\eta_R = \left| \frac{1}{2}(t_x - t_y e^{i\phi}) \left| \vec{E}_{in} \left| \vec{L} \right\rangle \right|^2$, $\eta_L = \left| \frac{1}{2}(t_x - t_y e^{i\phi}) \left| \vec{E}_{in} \left| \vec{R} \right\rangle \right|^2$, with η_E, η_R, η_L being the polarization order coupling efficiencies. $\langle \bullet | \bullet \rangle$ denotes the inner

product and $\left| \vec{R} \right\rangle \left\langle \vec{L} \right|$ represents the RCP (LCP) component. t_x and t_y are the amplitude of the transmission coefficient for the linear polarization perpendicular and parallel to the optical axis (i.e., parallel to the x - and y -axis, respectively), when $\varphi = 0$, with φ being the phase difference between the transmission coefficients. When the incident wave is purely RCP (or LCP), the efficiency η_R (or η_L) vanishes, and Equation (1) indicates that the transmitted field from a PB element comprises two polarization orders. One maintains the phase and original polarization state of the incident wave, while the other exhibits the opposite handedness and a phase modification of $\pm 2\theta$, where the ' \pm ' sign corresponds to both the rotating direction of the unit cells and the handedness of the incident wave.

Several works have appeared dedicated to holograms based on PB phase metasurfaces [48–51]. For example, as shown in Figure 1a, Wen et al. [48] used two sets of reflective PB phase metasurfaces, which consist of a two-dimensional array of elongated silver nanorods with a spacer layer of quartz (SiO₂) and a silver background layer with a thickness of 150 nm on a silicon substrate. When the helicity of the incident light is reversed, the staggered nanorod array realizes the position exchange of the reconstructed symmetrical holographic image in order to achieve spin multiplexing, in which the conversion efficiency can reach more than 40% in the range of 620 ~ 1020 nm. On the other hand, Khorasaninejad et al. [49] used geometric metasurfaces to transmit different letters in the same direction under different incident CP waves. Under circularly polarized incidence, the desired phase distribution was encoded into a directional rotating anisotropic nano-antenna array [50]. By designing the PB phase profile of the gold nanorod array with different orientation angles on the glass substrate, a 3D holographic image was realized (Figure 1b). In order to overcome the efficiency issue, Zheng et al. showed that a multilayered design of a reflective metasurface considerably improves the efficiency of the surface [51]. Similar to the concept of a metasurface-based reflective half-wave plate, the resonance of each nanorod was designed as a π -phase delay between two orthogonal linear axes in order to optimize the conversion efficiency between the two circularly polarized (CP) states. The diffraction efficiency exceeds 50% for a wide wavelength range of 630–1050 nm, and the maximum value can reach 80% at 825 nm, considering ohmic losses of metal at visible and near-infrared frequencies. In addition, there have also been many research studies on holographic imaging with phase-only control algorithms [52,53]. The advantage of these geometric metasurface holograms is that they are very robust against fabrication errors. the hologram is capable of tolerating a fabrication imperfection of up to 10% noise, which comprises the shape deformation of the rectangular aperture as well as the phase noise (Figure 1c) [52]. Figure 1d shows the simulated phase variations versus the orientation angle at the wavelengths of $\lambda = 633, 532, 488$ nm at equal intervals of $\pi/16$, respectively. Clearly, the modulation phases are linearly related to the orientation angle. The diffraction efficiency and image fidelity are asymptotically improved with the number of phase steps [53]. It is worth mentioning that a phase-only hologram consisting of plasmonic antennas operating in the near infrared using the weighted Gerchberg–Saxton (GS) algorithm has been theoretically studied [54].

Light is characterized by multiple properties, such as amplitude and phase. Therefore, amplitude information also plays an important role in the holography of light field regulation. Overvig et al. [55] modified the GS algorithm to impose a grayscale amplitude distribution instead of the conventional uniform amplitude distribution, in order to iteratively recover the phase required to produce a target holographic image at the object plane. A complex device with the desired functions can be realized by modulating the phase and amplitude information simultaneously. Some attempts have been made to achieve complex-amplitude modulation [56–63]. Ni et al. [57] demonstrated the use of nanostructured V-shaped antennas for amplitude and phase modulations at visible wavelengths, and their experimental results proved that the plasma metasurface modulates both the amplitude and phase distributions to produce a feasible way to generate holograms. Nanoantennas with other kinds of geometries, such as C-shaped antennas, can also be used to independently control the phase and amplitude of the cross-polarized wave [59].

Recent studies have shown that an X-shaped meta-atom [60] provides independent, continuous, broadband modulation of both the amplitude and phase information within the subwavelength scale. The maximum efficiency of a cross-polarized transmission achieves 49% at the wavelength of 532 nm. Moreover, the high-efficiency dielectric metasurface composed of birefringence meta-atoms with different rotation angles can simultaneously control the amplitude and phase at telecommunication frequencies for transmission-type devices [64]. The measured efficiency ranges from 72% to 97% depending on the exact design; such characteristics can realize most free-space transmissive optical elements. Wan et al. [65] demonstrated full-color ultrathin plasmonic metasurface holograms with both amplitude and phase modulations for the reconstruction of 2D and 3D holographic images with high resolution.

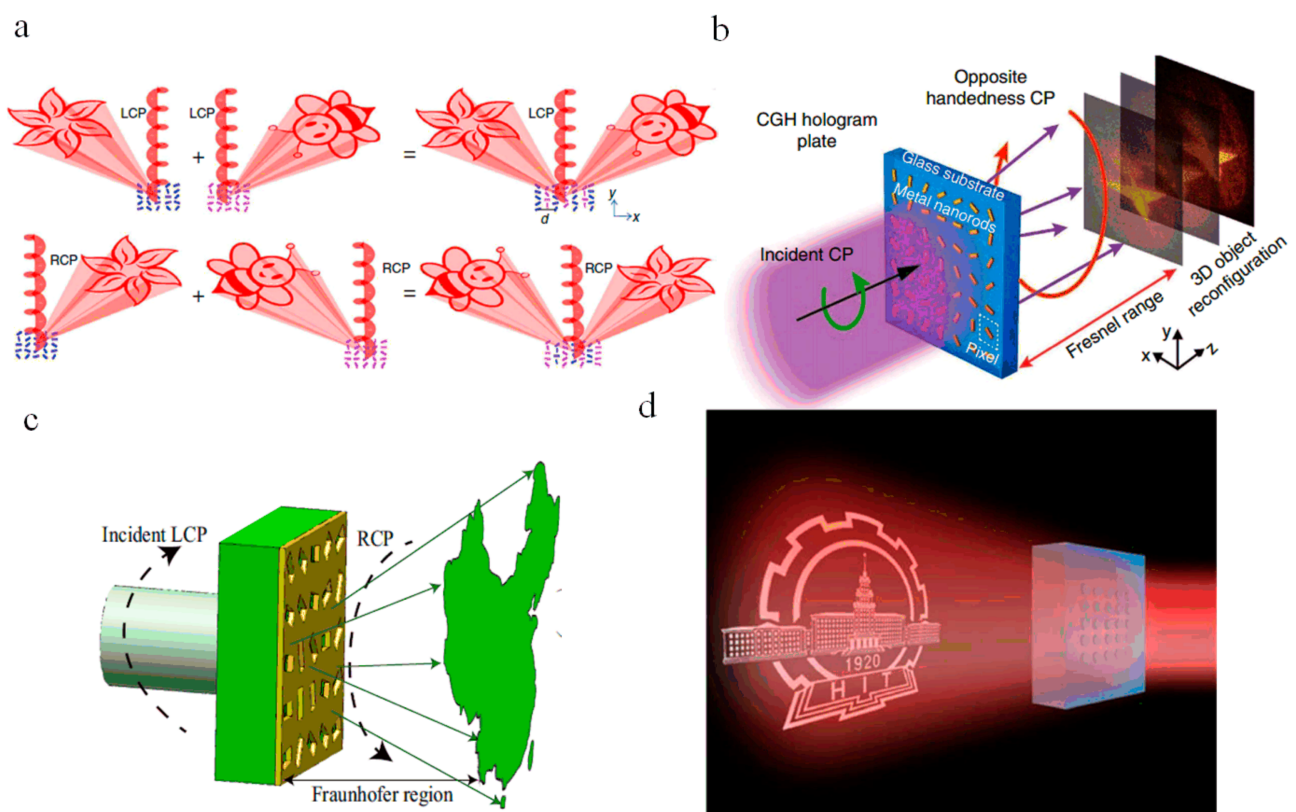


Figure 1. (a) Diagram of a helicity-multiplexed hologram realized by a reflective PB-phase metasurface. Reprinted with permission from ref. [48]. Copyright 2015 Springer Nature. (b) Transmissive-type three-dimensional optical holography by a plasmonic metasurface. Reprinted with permission from ref. [50]. Copyright 2013 Springer Nature. (c) A schematic diagram of the designed meta-hologram under LCP illumination and an image with RCP in the Fraunhofer region. Reprinted with permission from ref. [52]. Copyright 2016 Springer Nature. (d) An image of the Huygens' metasurface hologram. Reprinted with permission from ref. [53]. Copyright 2016 Springer Nature.

In order to enhance the capacity of information storage, the representative metasurface holographic multiplexing technologies include polarization multiplexing [66–72], wavelength multiplexing [73–76], angle multiplexing [77], spatial distribution multiplexing [78,79], orbital angular momentum (OAM) multiplexing [80–84], and so on. The polarization multiplexed metasurface holograms are sensitive to the incident polarization state, and can reconstruct different holographic images by switching the incident polarization. For example, a reflective-type and high-efficiency meta-hologram, which can achieve a four-level phase-modulation hologram for dual images under linearly polarized (LP) incident waves, is shown in Figure 2a [70]. It is worthwhile to note that Qiu and co-workers have introduced a dispersion-engineered metasurface with distinct functionalities con-

trolled by the wavelength. It has the same focal length for four different wavelengths in the spectrum. This work imposed a challenge of suppressing the cross-talk among multiple wavelengths without the help of extra spatial freedom [75]. In addition, Ren et al. proposed the metasurface, which can realize multi-channel orbital angular momentum holography. When the topological charge of the incident OAM beam is $l = -2, -1, 1, \text{ or } 2$, the multiplexed holographic technology can show the holographic images of different letters of "A", "B", "C", and "D", respectively, as shown in Figure 2b [80].

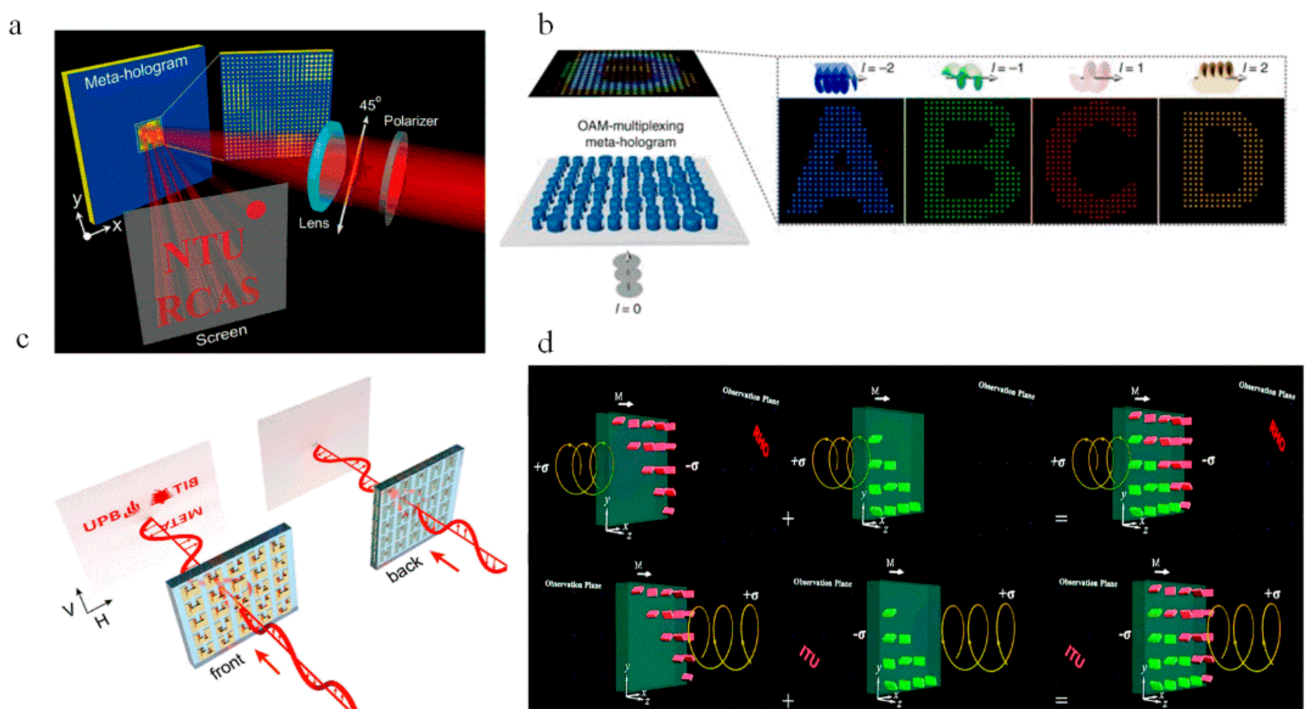


Figure 2. (a) Linear polarization multiplexing holography. Reprinted with permission from ref. [70]. Copyright 2014 American Chemical Society. (b) Schematic of an OAM-multiplexing meta-hologram capable of reconstructing multiple distinctive OAM-dependent holographic images. Adapted with permission from ref. [80]. Copyright 2019 Springer Nature. (c) Illustration of a double-layer metasurface with asymmetric functionalities. Reprinted with permission from ref. [85]. Copyright 2019 American Chemical Society. (d) The generation of direction-multiplexed metasurface holograms. Reprinted with permission from ref. [86]. Copyright 2019 Royal Society of Chemistry.

The concept of integrating holography and asymmetric light propagation has been further studied [85–88]. Illuminated by forward and backward propagating light, the metasurface behaves in a non-reciprocal manner, as shown in Figure 2c. In such a metasurface holographic system, a unique structural unit combined with a plasmon L-shaped nano-antenna and a plasmon dimer polarizer constitutes holographic information encoding, resulting in phase asymmetry in the propagation direction, which supports the directional encryption technology of holographic imaging [85]. In addition, for single-layer all-dielectric metasurfaces, direction multiplexing can also be achieved. Using rectangular nano-elements with two types of orientation shifts placed at different parts of the metasurface, CP light can be converted into cross-polarized light in different directions in order to achieve different images, "ITU" and "RHO", as displayed in Figure 2d [86], and the conversion efficiency is about 61%. Due to the construction of the modulation mechanism and structure, metasurface holography shows high flexibility and potential applications in the optical field, which can be used as a tool for practical engineering problems.

Field-vector holography, a fast-growing technique using metasurfaces, is exploited in order to overcome the limitation on the polarization insensitivity of some natural materials, and thus to realize vectorial holography. For example, by changing the spatial

displacement and orientation angle of di-atoms, it was shown that the polarization state of the image can also be controlled [89]. In addition, the use of structurally birefringent dielectric metasurfaces to demonstrate vector holograms with almost any polarization mode has been explored. Converting the red-green-blue data in any color image into Stokes parameters proves that the displayed metasurface can store and project color image data in the polarization state of a monochromatic hologram [90]. Recently, Ren et al. [91] demonstrated 3D vectorial holography through the use of a machine learning inverse design based on multilayer perceptron artificial neural networks (MANN) for the time-efficient and accurate reconstruction of a 3D vectorial holographic image. The results provide an artificial intelligence-enabled holographic paradigm for harnessing the vectorial nature of light, enabling new machine learning strategies for holographic 3D vectorial fields multiplexing in display and encryption.

3. Microwave Metasurface Hologram

As discussed above, artificial electromagnetic surfaces can accurately regulate the amplitude, phase, and polarization states of electromagnetic waves in the sub-wavelength range, which provides the possibility of achieving high-resolution and high imaging efficiency holographic imaging technology. Most of the research studies on metasurface holographic imaging technologies are concentrated in the optical frequency regime. Since optical imaging requires high-precision processing requirements and high cost, as well as cumbersome equipment necessary to construct an imaging system, it is difficult to cope such technology with certain portable mobile systems, and therefore it is still far from industrial production. In contrast, fabrication techniques of metasurfaces in the microwave regime are relatively mature and simple, and have practical application value due to their low-cost, conformal and mass imaging requirements. Due to the particularity of the microwave operating bandwidth, holographic technology is useful for near-field electromagnetic wave signal transmissions [92], as illustrated in Figure 3, and other related applications [93–99].

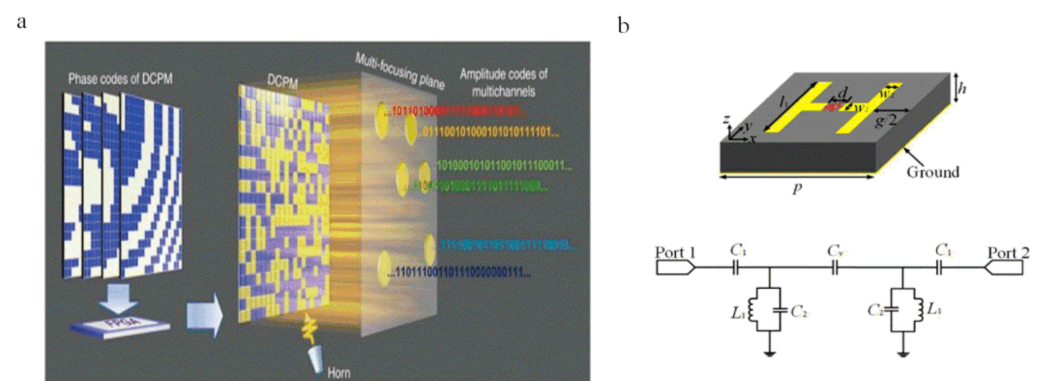


Figure 3. (a) Diagram of a multichannel transmission system in the near field region. Adapted with permission from ref. [92]. Copyright 2019 Springer Nature. (b) Unit cell loaded with a varactor diode. Reprinted with permission from ref. [93]. Copyright 2018 Optical Society of America.

3.1. Realization of Microwave Metasurface Holography

Through the optimization and design of each meta-atom of the metasurface, the phase control of electromagnetic waves can be realized. The PB phase metasurface is a type of structure that can continuously control the phase of electromagnetic waves by changing the rotation angle of the metasurface unit. As shown in Figure 4a for a reflective metasurface, the phase change can cover the whole range of 2π , while the amplitude of the reflection coefficient is maintained near unity, indicating that almost all of the incident energy can be transformed to the cross-polarized component. A holographic algorithm is utilized to calculate the phase distribution at the interface of the metamirror in order to achieve the

desired multi-focus spots. The proposed metamirror provides a high-performance solution for low-cost and lightweight beam-shaping and beam-focusing devices [100]. Additionally, as presented in Figure 4b, dual-polarized tri-channel encrypted holography is realized by a PB phase reflective metasurface when it is illuminated by an LP incident plane wave, which is appealing for applications in information encryption/storage [101]. In order to overcome the bulky profile due to the plane wave illumination, a low-profile holographic method was proposed using a leaky-type 2-bit coding Fabry–Perot metasurface with in-plane feeding in the microwave domain. In such a structure, the position of the resonance point only requires a slight change in the size of the unit structure to cause a sharp shift in phase. Considering the influence of the transmission phase of the partially reflective surface, the traditional optical ray model was modified in consequence. More importantly, this design overcomes the shortcoming of the bulky profile, and it constitutes the first work to achieve 2D functions from metasurfaces in a leaky-mode mechanism [102]. In 2020, Cui et al. proposed to synthesize the amplitude and phase in the region of interest simultaneously and independently utilizing high-efficiency phase-only metasurfaces [103]. An efficient method based on an equivalent electromagnetic model and gradient-based nonlinear optimization was proposed. Full-wave simulations and experimental results demonstrate that the phase-only metasurface designed by the method has 10 times higher efficiency than the phase-amplitude-modulated metasurface. This work opened a way to realize more complicated and high-efficiency metasurface holography.

Huygens' metasurface is a planar meta-atom array composed of crossed electric and magnetic dipoles, which provide a specific surface current to tailor the electromagnetic field distribution. According to the equivalence principle and boundary conditions, arbitrary reflection and transmission coefficients can be realized with specific surface electromagnetic impedance [104]:

$$Z_e = \frac{\eta}{2} \frac{1 + (R + T)}{1 - (R + T)} \quad (2)$$

$$Z_m = 2\eta \frac{1 + (R - T)}{1 - (R - T)} \quad (3)$$

where $R = re^{j\phi_r}$ and $T = te^{j\phi_t}$ represent the reflection and transmission coefficients, respectively. According to Equation (3), the required surface electrical impedance Z_e and magnetic impedance Z_m can be obtained using the given transmission and reflection coefficients. In 2018, following the developments of Huygens' metasurface with complete phase shift coverage, Wang et al. proposed a novel Huygens' metasurface hologram at microwave frequencies with detailed studies on the electromagnetic field distribution of the metasurface hologram for the imaging and modulation of the energy distribution among the focal points [105]. This proposed Huygens' metasurface extends the approach of holographic microwave applications, as shown in Figure 5a. The experiments show the hologram images with 89% transmittance efficiency, and 59% imaging efficiency. Upon efficient full-phase control, a polarization selector can be applied to holographic imaging technology in order to achieve two independent electromagnetic wave control effects under orthogonally LP incident waves, effectively increasing the storage capacity of the image information on a single Huygens' surface, and providing a precise and efficient simple solution for multi-channel transmissions without introducing any adjustable devices [106]. In addition, the working frequency band of the Huygens' surface was broadened in order to solve the shortcomings of the narrow operating frequency band in resonant artificial electromagnetic surfaces. Wang et al. also proposed and experimentally validated a 3D holographic imaging technique utilizing a broadband Huygens' metasurface, as shown in Figure 5b [107]. By modulating the overlap of the electric and magnetic resonances, 16 Huygens' meta-atoms with a 2π transmission-phase range were arranged to produce the phase profile obtained by the modified holographic weighted Gerchberg–Saxton (GSW) algorithm. This article realizes 10–14 GHz 3D holographic imaging, and increases the bandwidth; the solution still guarantees its advantages of high resolution and high imag-

ing efficiency, and summarizes the changes in broadband imaging characteristics with frequency, which is an important reference for its practical engineering application value.

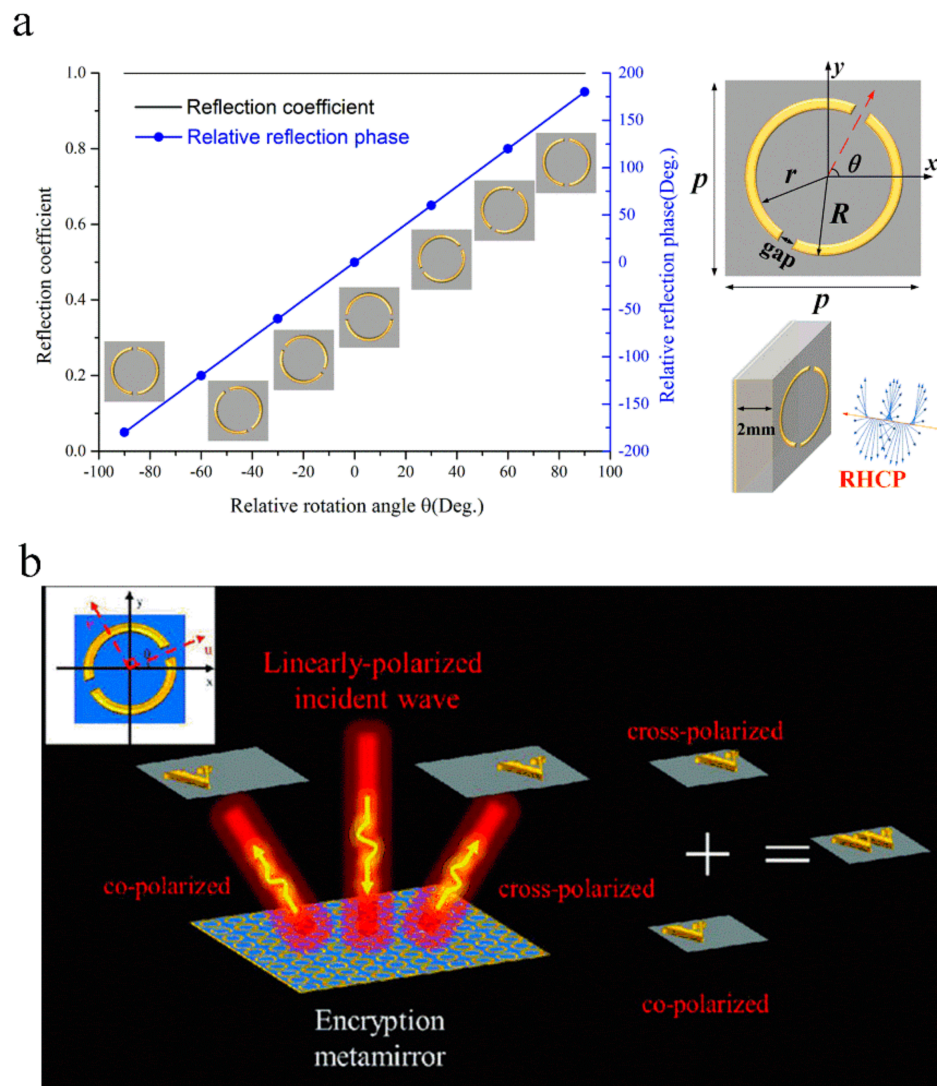


Figure 4. (a) Numerical characterization results of reflection-type PB phase elements. Reprinted with permission from ref. [100]. Copyright 2019 Optical Society of America. (b) Schematic representation of the proposed geometric phase metasurface-based dual-polarized tri-channel encrypted holography. Reprinted with permission from ref. [101]. Copyright 2020 John Wiley and Sons.

Based on the basic characteristics of Fourier transform, the Huygens’ surface can be modulated to control the holographic image. According to the surface antenna theory, the electric field distribution of the Huygens’ surface in the Cartesian coordinate system and the scattering electric field distribution function in the spherical coordinate system share a Fourier transform relationship. Therefore, this metasurface resorts to the properties of the Fourier transform to rotate and spatially project a holographic image towards desired elevation and azimuth angles, as shown in Figure 5c [108]. The schematic diagram of the spatial rotation operation based on the reflective Huygens’ metasurface is shown in Figure 5d [109]. The predesigned rotation angle in the plane or in a specific direction in space with negligible distortion to an original pattern can be achieved.

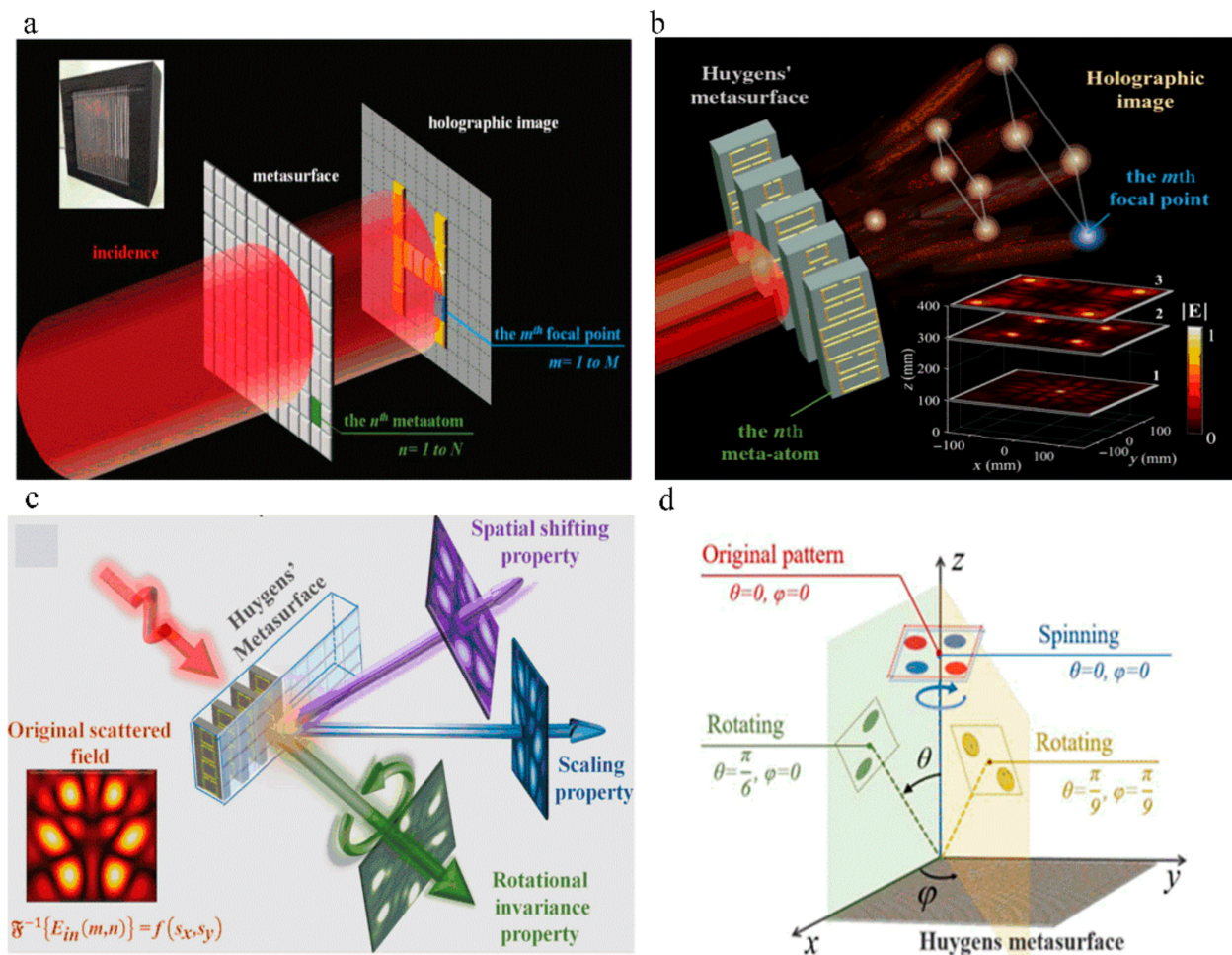


Figure 5. Huygens’ metasurface design and some application examples. (a) Schematic diagram of the proposed Huygens’ metasurface hologram for imaging with the desired focal intensity distribution. Reprinted with permission from ref. [105]. Copyright 2018 John Wiley and Sons. A photograph of the fabricated sample is shown in the upper left insert. (b) Illustration of the hologram structure and the reconstruction procedure of the microwave 3D imaging utilizing Huygens’ metasurface. Reprinted with permission from ref. [107]. Copyright 2020 American Physical Society. (c) A frequency-domain modulating metasurface performing Fourier transform properties. Adapted with permission from ref. [108]. Copyright 2020 Springer Nature. (d) Schematic diagram of the spatial rotation operations. Reprinted with permission from ref. [109]. Copyright 2019 IEEE.

3.2. Polarization-Multiplexed Metasurface Holograms

Polarization multiplexed metasurface holograms are sensitive to the incident polarization state, and different holographic images can be reconstructed by changing the incident wave polarization. For the transmission-type metasurface [110], the coding metasurface holographic can project two independent holographic images at the same time under a unique linearly polarized incidence, while avoiding crosstalk between the two different channels. The metasurface is composed of double-layer split-ring sub-wavelength elements, and the orientation of the double-layer split-ring aperture is specially designed to be 45° or 135°. A group of four digital elements is extracted in order to construct the 1-bit coding meta-hologram. The improved GSW algorithm is used to calculate the interface phase distribution in order to achieve identical multiplexed functionality for both the transmitted co- and cross-polarized components. A bilayer spin-decoupled information metasurface, shown in Figure 6a, has also been designed as an ultrathin structure with the amplitude of cross-polarization transmittance higher than 0.8 [111]. In this case, the incidence could be an RCP or LCP wave encoded with code “0” or “1”. The spin-decoupled design was

creatively combined with diffuse scattering and holographic technology in order to achieve different functionalities for corresponding circularly polarized channels.

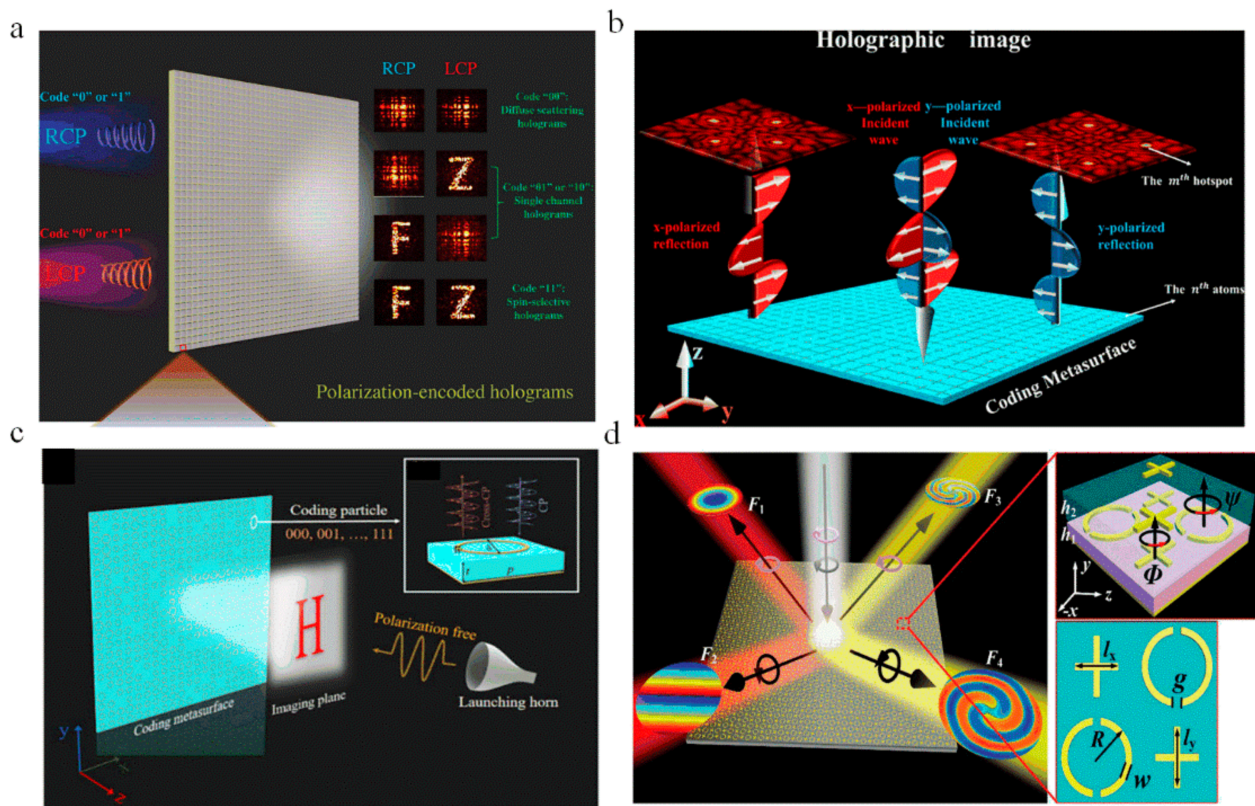


Figure 6. Polarization-multiplexed metasurface holograms. (a) A spin-selective transmission polarization-encoded hologram. Reprinted with permission from ref. [111]. Copyright 2020 John Wiley and Sons. (b) A co-polarization reflection coded hologram under the incidence of x - and y -polarized plane waves. Reprinted with permission from ref. [112]. Copyright 2021 AIP Publishing. (c) A helicity-switched meta-hologram that reflects the letter H under the incidence of a circularly polarized wave. Reprinted with permission from ref. [113]. Copyright 2020 Optical Society of America. (d) Illustration of the quad-port meta-plexer using the proposed mode- and spin-decoupled meta-atom. Reprinted with permission from ref. [114]. Copyright 2019 John Wiley and Sons.

For the reflective metasurface displayed in Figure 6b, Shang et al. [112] proposed a reflection-type 2-bit coding metasurface for polarization-multiplexed holograms in the microwave regime. The designed coding metasurface, as a double-layer meta-atom array composed of two cross-type metal patches, can realize the independent control of orthogonally polarized reflected waves, such that the meta-hologram can present different images under orthogonally linearly polarized incidences. As shown in Figure 6c [113], the proposed design not only allows us to overcome anti-symmetrical response characteristics between cross-circularly polarized states to enable the achievement of identical functionality under both RCP and LCP wave illuminations without polarization-conversion losses but also offers an additional degree of freedom in the control of the handedness.

3.3. Frequency-Multiplexed Metasurface Holograms

Another widely used multiplexing technique for microwave holography is frequency-multiplexing [114–116]. A multifunctional metasurface created by multiplexing the frequency and wavevector was proposed, as illustrated in Figure 6d. By integrating both geometric and dynamic phases in split-ring resonators and crossbars in a chessboard configuration, the inherent limitation of spin-flipped PB phases can be completely decoupled between two spin states. The metasurface implemented spin-, frequency-, and wavevector-

dependent anomalous reflections, lensing, orbital angular momentum generation, and wavevector-multiplexed vortex scattering, along with two-dimensional holograms. Moreover, the high efficiency and image quality were guaranteed by suppressing both the angular and spin crosstalks [114].

In addition, it is worthwhile to note that Cui and co-workers have experimentally demonstrated that any two desired holographic images can be generated at the lower and higher frequency bands at the same time with only a single 2-bit coding metasurface. By modifying the geometry of each reflective coding particle, the corresponding phase response can be obtained. In order to obtain uniform field intensities, the GSW retrieval algorithm was utilized to extract the coding masks of the coding meta-holograms, and the imaging efficiency and the root-mean-square error (RMSE) merits verify the high image qualities [115]. In addition, a tri-layered high-efficiency transmissive metasurface that can achieve, simultaneously, multifunctional electromagnetic wave manipulation and frequency multiplexing was proposed in reference [116].

3.4. Space Asymmetric Propagation Hologram

Recently, full-space metasurfaces with a multilayer configuration have been used to achieve the two spatial mode control of a linearly polarized wave [117–119]. A recent approach further demonstrated that the full-space manipulation of electromagnetic waves can be achieved by the interleaved design of few-layer metasurfaces, as illustrated in Figure 7a [119]. The basic unit cell design based on the scattering matrix theory enables the realization of the unidirectional transmission of electromagnetic waves with phase control, such as one-way anomalous refraction and one-way focusing. By introducing a rotational twist in geometry, asymmetric transmission with the desired phase function has also been realized. Furthermore, by arranging these two types of unit cells in an interleaved manner, i.e., with a 90° twisted angle between two neighboring unit cells, distinct directional holograms can be obtained, as shown in Figure 7b. Their broken out-of-plane symmetry realized different functions for opposite propagation directions, enabling direction-dependent versatile functionalities and offering unprecedented possibilities for the asymmetric and full-space manipulation of electromagnetic waves.

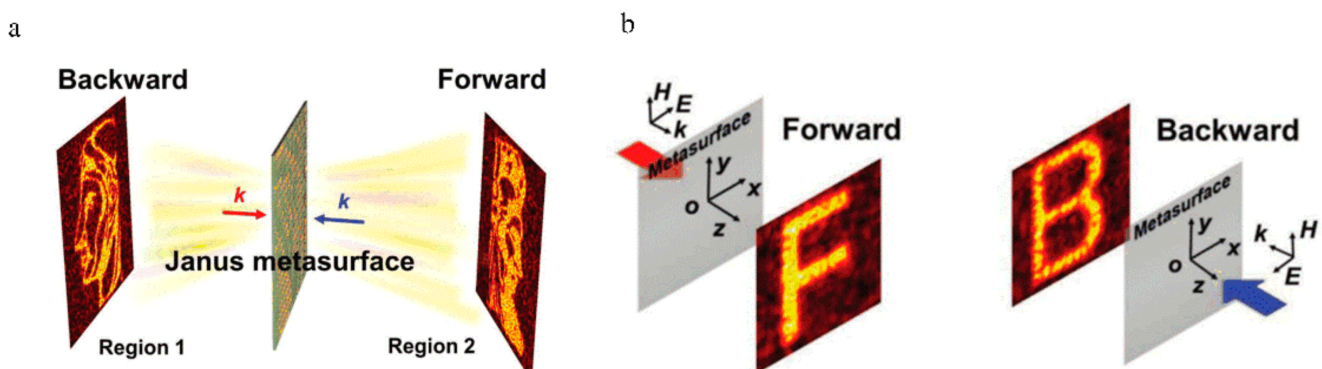


Figure 7. (a) Illustration of a Janus metasurface with bidirectional transmission for full-space wave manipulation. Adapted with permission from ref. [119]. Copyright 2019 John Wiley and Sons. (b) The incident wave forms different holograms for the two different propagation directions. Adapted with permission from ref. [119]. Copyright 2019 John Wiley and Sons.

3.5. Reconfigurable Metasurface Holograms

For tunable metasurfaces loaded by diodes, the electromagnetic response characteristics can be dynamically controlled by adjusting the applied bias voltage on the electronic components. In 2017, Chen et al. achieved electromagnetic response characteristic tuning by biasing the voltage on each cell in a reconfigurable metasurface array loaded with varactor diodes [120]. Multiple complex focal spots were simultaneously controlled at different spatial positions (Figure 8a), and the total focusing efficiency reached $\approx 36\%$.

Recently, a reconfigurable holographic metamirror implementing the proper phase-profile distribution necessary to dynamically control the focal spot was designed. The spatial energy distribution is manipulated in order to control the incident plane wave and create an adaptive focusing mechanism whereby both the number and position of focal spots can be modified [121].

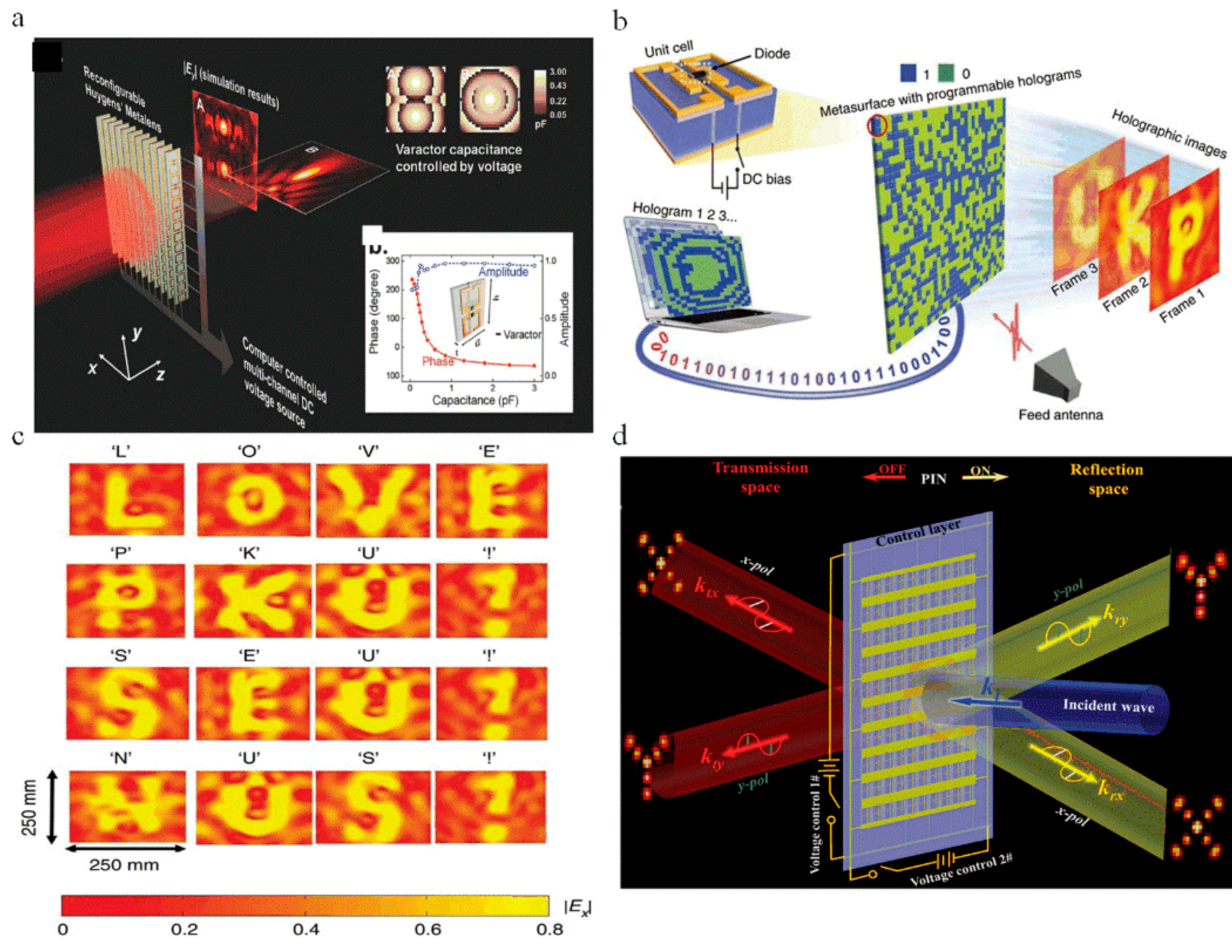


Figure 8. A variety of electrically reconfigurable metasurface designs. (a) Loaded with diodes for focal length control. Reprinted with permission from ref. [120]. Copyright 2017 John Wiley and Sons. (b) The schematic of a holographic imaging system based on microwave programmable coding metasurfaces. Reprinted with permission from ref. [122]. Copyright 2017 Springer Nature. (c) The experimental results of hologram images. Reprinted with permission from ref. [122]. Copyright 2017 Springer Nature. (d) Anisotropic digitally coded metasurface with the independent control of the transmission and reflection modes under x and y polarized incidence. Reprinted with permission from ref. [123]. Copyright 2020 John Wiley and Sons.

Furthermore, a dynamic holographic system based on a 1-bit programmable metasurface was developed at microwave frequencies [122]. Figure 8b shows the operating principle of such a holographic imaging system. It can be observed that the constitutive elements of the programmable metasurface incorporate real-time switchable encoding states, and that they can be independently controlled on a two-dimensional (2D) scale. By incorporating a $p-i-n$ diode into the metasurface cell, the scattering state of each individual cell can be controlled by applying two different bias voltages for the 'ON' and 'OFF' states of the diode. Therefore, a single metasurface can dynamically perform various functions through a field-programmable gate array (FPGA) program control. Due to the sub-wavelength characteristics of metasurface elements, holographic images with high resolution are achieved, as shown in Figure 8c. Another $p-i-n$ diode loaded reconfigurable anisotropic has been proposed to independently control not only the near/far-field pattern

but also the reflection and transmission modes of different incident electromagnetic wave polarizations, as shown in Figure 8d [123]. Both the numerical simulations and experimental measurements show that different holographic images can be achieved under vertical and horizontal linear polarizations, respectively, and that operation in the transmission mode or reflection mode can be controlled in real-time.

4. Perspective in Metasurface Holography

The metasurface holography demonstrated so far possesses high design flexibility owing to its diverse modulation mechanisms and structural building blocks. The holography principle is used as a tool to solve an inverse engineering problem in order to excite either free-space beams or surface waves with any desirable field distribution. Nevertheless, several challenges remain, such as the utilization of high-permittivity all-dielectric metasurfaces in order to avoid metal losses for high efficiency, enlarging the device diameter of the metasurface for high NA and resolution, and designing meta-atom structures of nanodisks (or nanorods) for polarization-insensitive (or polarization-sensitive) wavefront control. Besides this, there is still room for the advancement of metasurface holography by integrating reconfigurable metasurfaces into hologram designs, paving the way for future applications, including tunable optical imaging, high-capacity information storage, multiple-channel communication, and multi-mode pattern recognition. Different metasurface designs can achieve different functionalities and characteristics. As such, the expansion of metasurfaces in other fields will be an important goal for further exploration in the future.

5. Conclusions

Metasurfaces provide a good platform to realize holograms with high performances due to the capabilities of fully manipulating the amplitude, phase and polarization of electromagnetic waves. This article reviews the history and development of metasurface holography, from the early generation of holographic images to the most recent advanced holographic multiplexing technology. We briefly presented the implementation of metasurfaces for holographic imaging in the optical field. For holographic imaging in the microwave regime, we reviewed the implementation of phase modulation, polarization multiplexing, frequency multiplexing, spatial asymmetric transmission, and reconfigurable metasurfaces. The main contributions in this research field were presented together with some demonstration results. Metasurfaces can provide simple and low-cost systems, along with high efficiency. Due to their design flexibility, adjustability and multi-functionality, metasurfaces can be widely implemented in various applications in the future.

Author Contributions: Conceptualization, X.D., K.Z. and S.N.B.; writing—original draft preparation, G.S. and Z.W.; writing—review and editing, X.D., H.L. and S.N.B.; supervision, X.D. and Q.W.; funding acquisition, X.D. All authors have read and agreed to the published version of the manuscript.

Funding: This research was funded by the National Natural Science Foundation of China, grant number 61701141, 61805057, and the Open project of State Key Laboratory of Millimeter Waves, grant number K202001.

Institutional Review Board Statement: Not applicable.

Informed Consent Statement: Not applicable.

Data Availability Statement: No new data were created or analyzed in this study. Data sharing is not applicable to this article.

Conflicts of Interest: The authors declare no conflict of interest.

References

1. Gabor, D. A new microscope principle. *Nature* **1948**, *161*, 777. [[CrossRef](#)]
2. Maiman, T.H. Stimulated Optical Radiation in Ruby. *Nature* **1960**. [[CrossRef](#)]
3. Gabor. Microscopy by Reconstructed Wave Fronts: II. *Proc. Phys. Soc.* **1951**, *64*, 449–469. [[CrossRef](#)]
4. Sirat, G.Y.; Paz, F.; Agronik, G. Conoscopic holography. *Proc. SPIE Int. Soc. Opt. Eng.* **2005**, *10*, 11–16.

5. Miao, J.; Charalambous, P.; Kirz, J. Extending the methodology of X-ray crystallography to allow imaging of micrometre-sized non-crystalline specimens. *Nature* **1999**, *400*, 342–344. [[CrossRef](#)]
6. Mertz, L.; Young, N.O. Fresnel transformations of images. *SPIE Milest. Ser. MS* **1996**, *128*, 44–49.
7. Kim, S.G.; Lee, B.; Kim, E.S. Resolution analysis of incoherent triangular holography. *Appl. Opt.* **2001**, *40*, 4672–4678. [[CrossRef](#)] [[PubMed](#)]
8. Rosen, J.; Brooker, G. Digital spatially incoherent Fresnel holography. *Opt. Lett.* **2007**, *32*, 912–914. [[CrossRef](#)]
9. Rosen, J.; Brooker, G. Fluorescence incoherent color holography. *Opt. Express* **2007**, *15*, 2244–2250. [[CrossRef](#)] [[PubMed](#)]
10. Vijayakumar, A.; Kashter, Y.; Kelner, R.; Rosen, J. Coded aperture correlation holography—A new type of incoherent digital holograms. *Opt. Express* **2016**, *24*, 12430–12441. [[CrossRef](#)]
11. Hong, J.; Kim, M.K. Resolution Enhancement of Incoherent Digital Holography using the Super Resolution Image Reconstruction Technique. In *Digital Holographic Optical Processing*; OSA Technical Digest (CD): Kohala Coast, HI, USA, 2013; p. DTh1A.3.
12. Siegel, N.; Storrie, B.; Bruce, M.; Brooker, G. CINCH (confocal incoherent correlation holography) super resolution fluorescence microscopy based upon FINCH (Fresnel incoherent correlation holography). *Proc. SPIE Int. Soc. Opt. Eng.* **2015**, 9336. [[CrossRef](#)]
13. Kim, M.K. Full color natural light holographic camera. *Opt. Express* **2013**, *21*, 9636–9642. [[CrossRef](#)]
14. Barbastathis, G.; Balberg, M.; Brady, D.J. Confocal microscopy with a volume holographic filter. *Opt. Lett.* **1999**, *24*, 811–813. [[CrossRef](#)]
15. Lohmann, A.W.; Paris, D.P. Binary Fraunhofer Holograms, Generated by Computer. *App. Opt.* **1967**, *6*, 1739–1748. [[CrossRef](#)]
16. Shimobaba, T.; Kakue, T.; Ito, T. Review of Fast Algorithms and Hardware Implementations on Computer Holography. *IEEE Trans. Ind. Inf.* **2016**, *12*, 1611–1622. [[CrossRef](#)]
17. Brown, B.R.; Lohmann, A.W. Complex Spatial Filtering with Binary Masks. *App. Opt.* **1966**, *5*. [[CrossRef](#)]
18. Hutton, G. Fast-Fourier-transform holography: Recent results. *Opt. Lett.* **1978**, *3*, 30–32. [[CrossRef](#)] [[PubMed](#)]
19. Faklis, D.; Michael, G. Spectral properties of multi order diffractive lenses. *App. Opt.* **1995**, *34*, 2462–2468. [[CrossRef](#)] [[PubMed](#)]
20. Barlev, O.; Golub, M.A. Multifunctional binary diffractive optical elements for structured light projectors. *Opt. Express* **2018**, *26*, 21092–21107. [[CrossRef](#)]
21. Roberts, D. Polarization-independent diffractive waveplate optics. In Proceedings of the 2018 IEEE Aerospace Conference, Big Sky, MT, USA, 3–10 March 2018.
22. Zhan, T.; Xiong, J.; Lee, Y.H. Polarization-independent Pancharatnam-Berry phase lens system. *Opt. Express* **2018**, *26*, 35026–35033. [[CrossRef](#)] [[PubMed](#)]
23. Zhang, L.; Mei, S.; Huang, K.; Qiu, C.W. Advances in Full Control of Electromagnetic Waves with Metasurfaces. *Adv. Opt. Mater.* **2016**, *4*, 818–833. [[CrossRef](#)]
24. Hsiao, H.-H.; Chu, C.H.; Tsai, D.P. Fundamentals and Applications of Metasurfaces. *Small Methods* **2017**, *1*. [[CrossRef](#)]
25. Ding, F.; Pors, A.; Bozhevolnyi, S.I. Gradient metasurfaces: A review of fundamentals and applications. *Rep. Prog. Phys.* **2017**, *81*, 26401. [[CrossRef](#)]
26. Chen, S.; Li, Z.; Zhang, Y.; Cheng, H.; Tian, J. Phase Manipulation of Electromagnetic Waves with Metasurfaces and Its Applications in Nanophotonics. *Adv. Opt. Mater.* **2018**, *6*. [[CrossRef](#)]
27. Sung, J.; Lee, G.-Y.; Lee, B. Progresses in the practical metasurface for holography and lens. *Nanophotonics* **2019**, *8*, 1701–1718. [[CrossRef](#)]
28. Genevet, P.; Capasso, F.; Aieta, F.; Khorasaninejad, M.; Devlin, R. Recent advances in planar optics: From plasmonic to dielectric metasurfaces. *Optica* **2017**, *4*, 139–152. [[CrossRef](#)]
29. Yang, Y.; Wang, W.; Moitra, P.; Kravchenko, I.I.; Briggs, D.P.; Valentine, J. Dielectric meta-reflectarray for broadband linear polarization conversion and optical vortex generation. *Nano Lett.* **2014**, *14*, 1394–1399. [[CrossRef](#)]
30. Huang, K.; Liu, H.; Restuccia, S.; Mehmood, M.Q.; Mei, S.T.; Giovannini, D.; Danner, A.; Padgett, M.J.; Teng, J.H.; Qiu, C.W. Spiniform phase-encoded metagratings entangling arbitrary rational-order orbital angular momentum. *Light. Sci. Appl.* **2018**, *7*. [[CrossRef](#)]
31. Chen, Y.; Yang, X.; Gao, J. Spin-Selective Second-Harmonic Vortex Beam Generation with Babinet-Inverted Plasmonic Metasurfaces. *Adv. Opt. Mater.* **2018**, *6*. [[CrossRef](#)]
32. Pégard, N.C.; Fleischer, J.W. Optimizing holographic data storage using a fractional Fourier transform. *Opt. Lett.* **2011**, *36*, 2551–2553. [[CrossRef](#)]
33. Goh, X.M.; Zheng, Y.; Tan, S.J.; Zhang, L.; Kumar, K.; Qiu, C.W.; Yang, J.K. Three-dimensional plasmonic stereoscopic prints in full colour. *Nat. Commun.* **2014**, *5*. [[CrossRef](#)]
34. Jin, L.; Dong, Z.; Mei, S.; Yu, Y.F.; Wei, Z.; Pan, Z.; Rezaei, S.D.; Li, X.; Kuznetsov, A.I.; Kivshar, Y.S.; et al. Noninterleaved Metasurface for (2(6)-1) Spin- and Wavelength-Encoded Holograms. *Nano Lett.* **2018**, *18*, 8016–8024. [[CrossRef](#)]
35. Liu, H.C.; Yang, B.; Guo, Q.; Shi, J.; Guan, C.; Zheng, G.; Mühlender, H.; Li, G.; Zentgraf, T.; Zhang, S. Single-pixel computational ghost imaging with helicity-dependent metasurface hologram. *Sci. Adv.* **2017**, *3*, e1701477. [[CrossRef](#)]
36. Chen, W.T.; Zhu, A.Y.; Sanjeev, V.; Khorasaninejad, M.; Shi, Z.; Lee, E.; Capasso, F. A broadband achromatic metalens for focusing and imaging in the visible. *Nat. Nanotechnol.* **2018**, *13*, 220–226. [[CrossRef](#)]
37. Wang, S.; Wu, P.C.; Su, V.C.; Lai, Y.C.; Chen, M.K.; Kuo, H.Y.; Chen, B.H.; Chen, Y.H.; Huang, T.T.; Wang, J.H.; et al. A broadband achromatic metalens in the visible. *Nat. Nanotechnol.* **2018**, *13*, 227–232. [[CrossRef](#)]

38. Wang, S.; Wu, P.C.; Su, V.C.; Lai, Y.C.; Hung Chu, C.; Chen, J.W.; Lu, S.H.; Chen, J.; Xu, B.; Kuan, C.H.; et al. Broadband achromatic optical metasurface devices. *Nat. Commun.* **2017**, *8*, 187. [[CrossRef](#)]
39. Ma, Z.; Li, Y.; Li, Y.; Gong, Y.; Maier, S.A.; Hong, M. All-dielectric planar chiral metasurface with gradient geometric phase. *Opt. Express* **2018**, *26*, 6067–6078. [[CrossRef](#)]
40. Pan, C.; Ren, M.; Li, Q.; Fan, S.; Xu, J. Broadband asymmetric transmission of optical waves from spiral plasmonic metamaterials. *Appl. Phys. Lett.* **2014**, *104*. [[CrossRef](#)]
41. Bao, Y.; Yu, Y.; Xu, H.; Lin, Q.; Wang, Y.; Li, J.; Zhou, Z.-K.; Wang, X.-H. Coherent Pixel Design of Metasurfaces for Multidimensional Optical Control of Multiple Printing-Image Switching and Encoding. *Adv. Funct. Mater.* **2018**, *28*. [[CrossRef](#)]
42. Minovich, A.E.; Miroshnichenko, A.E.; Bykov, A.Y.; Murzina, T.V.; Neshev, D.N.; Kivshar, Y.S. Functional and nonlinear optical metasurfaces. *Laser Photonics Rev.* **2015**, *9*, 195–213. [[CrossRef](#)]
43. Xiao, Y.; Qian, H.; Liu, Z. Nonlinear Metasurface Based on Giant Optical Kerr Response of Gold Quantum Wells. *ACS Photonics* **2018**, *5*, 1654–1659. [[CrossRef](#)]
44. Li, G.; Wu, L.; Li, K.F.; Chen, S.; Schlickriede, C.; Xu, Z.; Huang, S.; Li, W.; Liu, Y.; Pun, E.Y.B.; et al. Nonlinear Metasurface for Simultaneous Control of Spin and Orbital Angular Momentum in Second Harmonic Generation. *Nano Lett.* **2017**, *17*, 7974–7979. [[CrossRef](#)]
45. Hasman, E.; Kleiner, V.; Biener, G. Polarization dependent focusing lens by use of quantized Pancharatnam–Berry phase diffractive optics. *Appl. Phys. Lett.* **2003**, *82*, 328–330. [[CrossRef](#)]
46. Bomzon, Z.; Biener, G.; Kleiner, V. Space-variant Pancharatnam–Berry phase optical elements with computer-generated subwavelength gratings. *Opt. Lett.* **2002**, *27*, 1141–1143. [[CrossRef](#)]
47. Ding, X.; Monticone, F.; Zhang, K.; Zhang, L.; Gao, D.; Burokur, S.N.; de Lustrac, A.; Wu, Q.; Qiu, C.-W. Ultrathin Pancharatnam–Berry metasurface with maximal cross-polarization efficiency. *Adv. Mater.* **2015**, *27*, 1195–1200. [[CrossRef](#)] [[PubMed](#)]
48. Wen, D.; Yue, F.; Li, G.; Zheng, G.; Chan, K.; Chen, S.; Chen, M.; Li, K.F.; Wong, P.W.; Cheah, K.W.; et al. Helicity multiplexed broadband metasurface holograms. *Nat. Commun.* **2015**, *6*, 8241. [[CrossRef](#)]
49. Khorasaninejad, M.; Ambrosio, A.; Kanhaiya, P.; Capasso, F. Broadband and chiral binary dielectric meta-holograms. *Sci. Adv.* **2016**, *2*, e1501258. [[CrossRef](#)] [[PubMed](#)]
50. Huang, L.; Chen, X.; Mühlenbernd, H.; Zhang, H.; Chen, S.; Bai, B.; Tan, Q.; Jin, G.; Cheah, K.-W.; Qiu, C.-W.; et al. Three-dimensional optical holography using a plasmonic metasurface. *Nat. Commun.* **2013**, *4*, 4. [[CrossRef](#)]
51. Zheng, G.; Mühlenbernd, H.; Kenney, M.; Li, G.; Zentgraf, T.; Zhang, S. Metasurface holograms reaching 80% efficiency. *Nat. Nanotechnol.* **2015**, *10*, 308–312. [[CrossRef](#)]
52. Zhang, X.; Jin, J.; Wang, Y.; Pu, M.; Li, X.; Zhao, Z.; Gao, P.; Wang, C.; Luo, X. Metasurface-based broadband hologram with high tolerance to fabrication errors. *Sci. Rep.* **2016**, *6*. [[CrossRef](#)]
53. Zhao, W.; Jiang, H.; Liu, B.; Song, J.; Jiang, Y.; Tang, C.; Li, J. Dielectric Huygens’ Metasurface for High-Efficiency Hologram Operating in Transmission Mode. *Sci. Rep.* **2016**, *6*. [[CrossRef](#)]
54. Zhou, F.; Liu, Y.; Cai, W. Plasmonic holographic imaging with V-shaped nanoantenna array. *Opt. Express* **2013**, *21*, 4348–4354. [[CrossRef](#)] [[PubMed](#)]
55. Overvig, A.C.; Shrestha, S.; Malek, S.C.; Lu, M.; Stein, A.; Zheng, C.; Yu, N. Dielectric metasurfaces for complete and independent control of the optical amplitude and phase. *Light. Sci. Appl.* **2019**, *8*, 1–12. [[CrossRef](#)]
56. Jiang, Q.; Cao, L.; Huang, L.; He, Z.; Jin, G. A complex-amplitude hologram using an ultra-thin dielectric metasurface. *Nanoscale* **2020**, *12*, 24162–24168. [[CrossRef](#)]
57. Ni, X.; Kildishev, A.V.; Shalae, V.M. Metasurface holograms for visible light. *Nat. Commun.* **2013**, *4*. [[CrossRef](#)]
58. Liu, L.; Zhang, X.; Kenney, M.; Su, X.; Xu, N.; Ouyang, C.; Shi, Y.; Han, J.; Zhang, W.; Zhang, S. Broadband Metasurfaces with Simultaneous Control of Phase and Amplitude. *Adv. Mater.* **2014**, *26*, 5031–5036. [[CrossRef](#)]
59. Song, E.-Y.; Lee, G.-Y.; Park, H.; Lee, K.; Kim, J.; Hong, J.; Kim, H.; Lee, B. Compact Generation of Airy Beams with C-Aperture Metasurface. *Adv. Opt. Mater.* **2017**, *5*, 5. [[CrossRef](#)]
60. Lee, G.-Y.; Yoon, G.; Lee, S.-Y.; Yun, H.; Cho, J.; Lee, K.; Kim, H.; Rho, J.; Lee, B. Complete amplitude and phase control of light using broadband holographic metasurfaces. *Nanoscale* **2018**, *10*, 4237–4245. [[CrossRef](#)]
61. Wang, Q.; Zhang, X.; Xu, Y.; Gu, J.; Li, Y.; Tian, Z.; Singh, R.; Zhang, S.; Han, J.; Zhang, W. Broadband metasurface holograms: Toward complete phase and amplitude engineering. *Sci. Rep.* **2016**, *6*. [[CrossRef](#)]
62. Chong, K.E.; Wang, L.; Staude, I.; James, A.R.; Dominguez, J.; Liu, S.; Subramania, G.S.; Decker, M.; Neshev, D.N.; Brener, I.; et al. Efficient Polarization-Insensitive Complex Wavefront Control Using Huygens’ Metasurfaces Based on Dielectric Resonant Meta-atoms. *ACS Photonics* **2016**, *3*, 514–519. [[CrossRef](#)]
63. Song, X.; Huang, L.; Tang, C.; Li, J.; Li, X.; Liu, J.; Wang, Y.; Zentgraf, T. Selective Diffraction with Complex Amplitude Modulation by Dielectric Metasurfaces. *Adv. Opt. Mater.* **2018**, *6*. [[CrossRef](#)]
64. Arbabi, A.; Horie, Y.; Bagheri, M.; Faraon, A. Dielectric metasurfaces for complete control of phase and polarization with subwavelength spatial resolution and high transmission. *Nat. Nanotechnol.* **2015**, *10*, 937–943. [[CrossRef](#)]
65. Wan, W.; Gao, J.; Yang, X. Full-Color Plasmonic Metasurface Holograms. *ACS Nano* **2016**, *10*, 10671–10680. [[CrossRef](#)]
66. Chen, Y.; Yang, X.; Gao, J. Spin-controlled wavefront shaping with plasmonic chiral geometric metasurfaces. *Light. Sci. Appl.* **2018**, *7*, 1–10. [[CrossRef](#)]

67. Huang, L.; Mühlenbernd, H.; Li, X.; Song, X.; Bai, B.; Wang, Y.; Zentgraf, T. Broadband Hybrid Holographic Multiplexing with Geometric Metasurfaces. *Adv. Mater.* **2015**, *27*, 6444–6449. [[CrossRef](#)]
68. Zhang, X.; Yang, S.; Yue, W.; Xu, Q.; Zhang, W. Direct polarization measurement using a multiplexed Pancharatnam-Berry meta-hologram. *Optica* **2019**, *6*. [[CrossRef](#)]
69. Wang, B.; Dong, F.; Yang, D.; Song, Z.; Xu, L.; Chu, W.; Gong, Q.; Li, Y. Polarization-controlled color-tunable holograms with dielectric metasurfaces. *Optica* **2017**, *4*, 1368–1371. [[CrossRef](#)]
70. Chen, W.T.; Yang, K.-Y.; Wang, C.-M.; Huang, Y.-W.; Sun, G.; Chiang, I.-D.; Liao, C.Y.; Hsu, W.-L.; Lin, H.T.; Sun, S.; et al. High-Efficiency Broadband Meta-Hologram with Polarization-Controlled Dual Images. *Nano Lett.* **2014**, *14*, 225–230. [[CrossRef](#)]
71. Mueller, J.P.B.; Rubin, N.A.; Devlin, R.C.; Groever, B.; Capasso, F. Metasurface Polarization Optics: Independent Phase Control of Arbitrary Orthogonal States of Polarization. *Phys. Rev. Lett.* **2017**, *118*. [[CrossRef](#)]
72. Wei, Q.; Huang, L.; Li, X.; Liu, J.; Wang, Y. Broadband Multiplane Holography Based on Plasmonic Metasurface. *Adv. Opt. Mater.* **2017**, *5*, 5. [[CrossRef](#)]
73. Walther, B.; Helgert, C.; Rockstuhl, C.; Setzpfandt, F.; Eilenberger, F.; Kley, E.B.; Lederer, F.; Tünnermann, A.; Pertsch, T. Spatial and Spectral Light Shaping with Metamaterials. *Adv. Mater.* **2012**. [[CrossRef](#)]
74. Franklin, D.; Modak, S.; Vázquez-Guardado, A.; Safaei, A.; Chanda, D. Covert infrared image encoding through imprinted plasmonic cavities. *Light. Sci. Appl.* **2018**, *7*, 1–8. [[CrossRef](#)]
75. Shi, Z.; Khorasaninejad, M.; Huang, Y.-W.; Roques-Carmes, C.; Zhu, A.Y.; Chen, W.T.; Sanjeev, V.; Ding, Z.-W.; Tamagnone, M.; Chaudhary, K.; et al. Single-Layer Metasurface with Controllable Multiwavelength Functions. *Nano Lett.* **2018**, *18*, 2420–2427. [[CrossRef](#)]
76. Li, X.; Ren, H.; Chen, X.; Liu, J.; Li, Q.; Li, C.; Xue, G.; Jia, J.; Cao, L.; Sahu, A.; et al. Athermally photoreduced graphene oxides for three-dimensional holographic images. *Nat. Commun.* **2015**, *6*, 6984. [[CrossRef](#)]
77. Kamali, S.M.; Arbabi, E.; Arbabi, A.; Horie, Y.; Faraji-Dana, M.; Faraon, A. Angle-Multiplexed Metasurfaces: Encoding Independent Wavefronts in a Single Metasurface under Different Illumination Angles. *Phys. Rev. X* **2017**, *7*, 7. [[CrossRef](#)]
78. Deng, J.; Yang, Y.; Tao, J.; Deng, L.; Liu, D.; Guan, Z.; Li, G.; Li, Z.; Yu, S.; Zheng, G.; et al. Spatial Frequency Multiplexed Meta-Holography and Meta-Nanoprinting. *ACS Nano* **2019**, *13*, 9237–9246. [[CrossRef](#)] [[PubMed](#)]
79. Gao, H.; Wang, Y.; Fan, X.; Jiao, B.; Li, T.; Shang, C.; Zeng, C.; Deng, L.; Xiong, W.; Xia, J.; et al. Dynamic 3D meta-holography in visible range with large frame number and high frame rate. *Sci. Adv.* **2020**, *6*, eaba8595. [[CrossRef](#)]
80. Ren, H.; Briere, G.; Fang, X.; Ni, P.; Sawant, R.; Héron, S.; Chenot, S.; Vézian, S.; Damilano, B.; Brändli, V.; et al. Metasurface orbital angular momentum holography. *Nat. Commun.* **2019**, *10*, 1–8. [[CrossRef](#)] [[PubMed](#)]
81. Jin, L.; Huang, Y.W.; Jin, Z.; Devlin, R.C.; Dong, Z.; Mei, S.; Jiang, M.; Chen, W.T.; Wei, Z.; Liu, H.; et al. Dielectric multi-momentum meta-transformer in the visible. *Nat. Commun.* **2019**, *10*, 4789. [[CrossRef](#)] [[PubMed](#)]
82. Fang, X.; Ren, H.; Gu, M. Orbital angular momentum holography for high-security encryption. *Nat. Photonics* **2020**, *14*, 102–108. [[CrossRef](#)]
83. Zhou, H.; Sain, B.; Wang, Y.; Schlickriede, C.; Zhao, R.; Zhang, X.; Wei, Q.; Li, X.; Huang, L.; Zentgraf, T. Polarization-Encrypted Orbital Angular Momentum Multiplexed Metasurface Holography. *ACS Nano* **2020**, *14*, 5553–5559. [[CrossRef](#)] [[PubMed](#)]
84. Ren, H.; Fang, X.; Jang, J.; Bürger, J.; Rho, J.; Maier, S.A. Complex-amplitude metasurface-based orbital angular momentum holography in momentum space. *Nat. Nanotechnol.* **2020**, *15*, 948–955. [[CrossRef](#)]
85. Frese, D.; Wei, Q.; Wang, Y.; Huang, L.; Zentgraf, T. Nonreciprocal Asymmetric Polarization Encryption by Layered Plasmonic Metasurfaces. *Nano Lett.* **2019**, *19*, 3976–3980. [[CrossRef](#)] [[PubMed](#)]
86. Ansari, M.A.; Kim, I.; Rukhlenko, I.D.; Zubair, M.; Yerci, S.; Tauqeer, T.; Mehmood, M.Q.; Rho, J. Engineering spin and antiferromagnetic resonances to realize an efficient direction-multiplexed visible meta-hologram. *Nanoscale Horizons* **2019**, *5*, 57–64. [[CrossRef](#)]
87. Ansari, M.A.; Kim, I.; Lee, D.; Waseem, M.H.; Zubair, M.; Mahmood, N.; Badloe, T.; Yerci, S.; Tauqeer, T.; Mehmood, M.Q.; et al. A Spin-Encoded All-Dielectric Metahologram for Visible Light. *Laser Photonics Rev.* **2019**, *13*. [[CrossRef](#)]
88. Kim, T.; Yu, E.S.; Bae, Y.G.; Lee, J.; Kim, I.S.; Chung, S.; Lee, S.Y.; Ryu, Y.S. Asymmetric optical camouflage: Tuneable reflective colour accompanied by the optical Janus effect. *Light Sci. Appl.* **2020**, *9*, 175. [[CrossRef](#)]
89. Deng, Z.-L.; Deng, J.; Zhuang, X.; Wang, S.; Li, K.; Wang, Y.; Chi, Y.; Ye, X.; Xu, J.; Wang, G.P.; et al. Diatomic Metasurface for Vectorial Holography. *Nano Lett.* **2018**, *18*, 2885–2892. [[CrossRef](#)]
90. Arbabi, E.; Kamali, S.M.; Arbabi, A.; Faraon, A. Vectorial Holograms with a Dielectric Metasurface: Ultimate Polarization Pattern Generation. *ACS Photonics* **2019**, *6*, 2712–2718. [[CrossRef](#)]
91. Ren, H.; Shao, W.; Li, Y.; Salim, F.; Gu, M. Three-dimensional vectorial holography based on machine learning inverse design. *Sci. Adv.* **2020**, *6*, eaaz4261. [[CrossRef](#)]
92. Wan, X.; Zhang, Q.; Chen, T.Y.; Zhang, L.; Xu, W.; Huang, H.; Xiao, C.K.; Xiao, Q.; Cui, T.J. Multichannel direct transmissions of near-field information. *Light. Sci. Appl.* **2019**, *8*, 1–8. [[CrossRef](#)]
93. Kuang, Z.; Hao, Y.; Xumin, D.; Qun, W. Experimental validation of active holographic metasurface for electrically beam steering. *Opt. Express* **2018**, *26*. [[CrossRef](#)]
94. Yu, H.; Zhang, K.; Ding, X.; Wu, Q. A Dual-Beam Leaky-Wave Antenna Based on Squarely Modulated Reactance Surface. *Appl. Sci.* **2020**, *10*, 962. [[CrossRef](#)]

95. Elsherbiny, M.; Fathy, A.E.; Rosen, A.; Ayers, G.; Perlow, S.M. Holographic Antenna Concept, Analysis, and Parameters. *IEEE Trans. Antennas Propag.* **2004**, *52*, 830–839. [[CrossRef](#)]
96. Sutinjo, A.; Okoniewski, M.; Johnston, R.H. A Holographic Antenna Approach for Surface Wave Control in Microstrip Antenna Applications. *IEEE Trans. Antennas Propag.* **2010**, *58*, 675–682. [[CrossRef](#)]
97. Pandi, S.; Balanis, C.A.; Birtcher, C.R. Design of Scalar Impedance Holographic Metasurfaces for Antenna Beam Formation With Desired Polarization. *IEEE Trans. Antennas Propag.* **2015**, *63*, 3016–3024. [[CrossRef](#)]
98. Sutinjo, A.; Okoniewski, M. A Surface Wave Holographic Antenna for Broadside Radiation Excited by a Traveling Wave Patch Array. *IEEE Trans. Antennas Propag.* **2010**, *59*, 297–300. [[CrossRef](#)]
99. Martinez-Ros, A.J.; Gomez-Tornero, J.L.; Goussetis, G. Holographic Pattern Synthesis with Modulated Substrate Integrated Waveguide Line-Source Leaky-Wave Antennas. *IEEE Trans. Antennas Propag.* **2013**, *61*, 3466–3474. [[CrossRef](#)]
100. Wang, Y.; Guan, C.; Ding, X.; Zhang, K.; Ratni, B.; Burokur, S.N.; Gu, X.; Wu, Q. Multi-focus hologram utilizing Pancha-ratnam-Berry phase elements based metamirror. *Opt. Lett.* **2019**, *44*, 2189–2192. [[CrossRef](#)]
101. Wang, Y.; Guan, C.; Li, H.; Ding, X.; Zhang, K.; Wang, J.; Burokur, S.N.; Liu, J.; Wu, Q. Dual-Polarized Tri-Channel Encrypted Holography Based on Geometric Phase Metasurface. *Adv. Photonics Res.* **2020**, *1*, 2000022. [[CrossRef](#)]
102. Li, H.; Li, Y.B.; Shen, J.L.; Cui, T.J. Low-Profile Electromagnetic Holography by Using Coding Fabry–Perot Type Metasurface with In-Plane Feeding. *Adv. Opt. Mater.* **2020**, *8*. [[CrossRef](#)]
103. Wu, J.W.; Wang, Z.X.; Fang, Z.Q.; Liang, J.C.; Fu, X.; Liu, J.F.; Wu, H.T.; Bao, D.; Miao, L.; Zhou, X.Y.; et al. Full-State Synthesis of Electromagnetic Fields using High Efficiency Phase-Only Metasurfaces. *Adv. Funct. Mater.* **2020**, *30*, 30. [[CrossRef](#)]
104. Zhu, B.O.; Feng, Y. Passive Metasurface for Reflectionless and Arbitrary Control of Electromagnetic Wave Transmission. *IEEE Trans. Antennas Propag.* **2015**, *63*, 5500–5511. [[CrossRef](#)]
105. Wang, Z.; Ding, X.; Zhang, K.; Ratni, B.; Burokur, S.N.; Gu, X.; Wu, Q. Huygens Metasurface Holograms with the Modulation of Focal Energy Distribution. *Adv. Opt. Mater.* **2018**, *6*. [[CrossRef](#)]
106. Ding, X.; Wang, Z.; Liu, S.; Zhang, K.; Wu, Q. Polarization-multiplexed Huygens metasurface holography. *Opt. Lett.* **2020**, *45*, 5488–5491. [[CrossRef](#)]
107. Wang, Z.; Liu, J.; Ding, X.; Zhao, W.; Zhang, K.; Li, H.; Ratni, B.; Burokur, S.N.; Wu, Q. Three-Dimensional Microwave Holography Based on Broadband Huygens' Metasurface. *Phys. Rev. Appl.* **2020**, *13*, 13. [[CrossRef](#)]
108. Ding, X.; Wang, Z.; Hu, G.; Liu, J.; Zhang, K.; Li, H.; Ratni, B.; Burokur, S.N.; Wu, Q.; Tan, J.; et al. Metasurface holographic image projection based on mathematical properties of Fourier transform. *Photonix* **2020**, *1*, 1–12. [[CrossRef](#)]
109. Ding, X.; Wang, Z.; Guan, C.; Liu, S.; Zhang, K.; Gu, X.; Wu, Q. Spatial Rotation Operations on Huygens Metasurface Hologram in Microwave Regime. *IEEE Trans. Magn.* **2019**, *55*, 1–4. [[CrossRef](#)]
110. Guan, C.; Liu, J.; Ding, X.; Wang, Z.; Zhang, K.; Li, H.; Jin, M.; Burokur, S.N.; Wu, Q. Dual-polarized multiplexed meta-holograms utilizing coding metasurface. *Nanophotonics* **2020**, *9*, 3605–3613. [[CrossRef](#)]
111. Wang, Z.X.; Wu, J.W.; Wu, L.W.; Gou, Y.; Ma, H.F.; Cheng, Q.; Cui, T.J. High Efficiency Polarization-Encoded Holograms with Ultrathin Bilayer Spin-Decoupled Information Metasurfaces. *Adv. Opt. Mater.* **2020**, *9*. [[CrossRef](#)]
112. Shang, G.; Li, H.; Wang, Z.; Zhang, K.; Burokur, S.N.; Liu, J.; Wu, Q.; Ding, X.; Ding, X. Coding metasurface holography with polarization-multiplexed functionality. *J. Appl. Phys.* **2021**, *129*. [[CrossRef](#)]
113. Guan, C.; Ding, X.; Wang, Z.; Zhang, K.; Jin, M.; Burokur, S.N.; Wu, Q. Helicity-switched hologram utilizing a polarization-free multi-bit coding metasurface. *Opt. Express* **2020**, *28*, 22669–22678. [[CrossRef](#)]
114. Xu, H.; Hu, G.; Jiang, M.; Tang, S.; Wang, Y.; Wang, C.; Huang, Y.; Ling, X.; Liu, H.; Zhou, J. Wavevector and Frequency Multiplexing Performed by a Spin-Decoupled Multichannel Metasurface. *Adv. Mater. Technol.* **2019**, *5*, 5. [[CrossRef](#)]
115. Iqbal, S.; Rajabalipanah, H.; Zhang, L.; Qiang, X.; Abdolali, A.; Cui, T.J. Frequency-multiplexed pure-phase microwave meta-holograms using bi-spectral 2-bit coding metasurfaces. *Nanophotonics* **2020**, *9*, 703–714. [[CrossRef](#)]
116. Sun, Q.; Zhang, Z.; Huang, Y.; Ma, X.; Pu, M.; Guo, Y.; Li, X.; Luo, X. Asymmetric Transmission and Wavefront Manipulation toward Dual-Frequency Meta-Holograms. *ACS Photonics* **2019**, *6*, 1541–1546. [[CrossRef](#)]
117. Zhang, L.; Wu, R.Y.; Bai, G.D.; Wu, H.T.; Ma, Q.; Chen, X.Q.; Cui, T.J. Transmission-Reflection-Integrated Multifunctional Coding Metasurface for Full-Space Controls of Electromagnetic Waves. *Adv. Funct. Mater.* **2018**, *28*. [[CrossRef](#)]
118. Zhang, C.; Wang, G.; Xu, H.X.; Zhang, X.; Li, H.P. Helicity-Dependent Multifunctional Metasurfaces for Full-Space Wave Control. *Adv. Opt. Mater.* **2020**, *8*. [[CrossRef](#)]
119. Chen, K.; Ding, G.; Hu, G.; Jin, Z.; Zhao, J.; Feng, Y.; Jiang, T.; Alù, A.; Qiu, C. Directional Janus Metasurface. *Adv. Mater.* **2019**, *32*, e1906352. [[CrossRef](#)] [[PubMed](#)]
120. Chen, K.; Feng, Y.; Monticone, F.; Zhao, J.; Zhu, B.; Jiang, T.; Zhang, L.; Kim, Y.; Ding, X.; Zhang, S.; et al. A Reconfigurable Active Huygens' Metalens. *Adv. Mater.* **2017**, *29*, 29. [[CrossRef](#)]
121. Ratni, B.; Wang, Z.; Zhang, K.; Ding, X.; de Lustrac, A.; Piau, G.-P.; Burokur, S.N. Dynamically Controlling Spatial Energy Distribution with a Holographic Metamirror for Adaptive Focusing. *Phys. Rev. Appl.* **2020**, *13*. [[CrossRef](#)]
122. Li, L.; Jun Cui, T.; Ji, W.; Liu, S.; Ding, J.; Wan, X.; Bo Li, Y.; Jiang, M.; Qiu, C.W.; Zhang, S. Electromagnetic reprogrammable coding-metasurface holograms. *Nat. Commun.* **2017**, *8*, 197. [[CrossRef](#)]
123. Wu, L.W.; Ma, H.F.; Wu, R.Y.; Xiao, Q.; Gou, Y.; Wang, M.; Wang, Z.X.; Bao, L.; Wang, H.L.; Qing, Y.M.; et al. Transmission-Reflection Controls and Polarization Controls of Electromagnetic Holograms by a Reconfigurable Anisotropic Digital Coding Metasurface. *Adv. Opt. Mater.* **2020**, *8*. [[CrossRef](#)]